Equivalence of pyrheliometric and monochromatic aerosol optical depths at a single key wavelength

Benoît Molineaux, Pierre Ineichen, and Norm O'Neill

The atmospheric aerosol optical depth (AOD) weighted over the solar spectrum is equal to the monochromatic AOD at a certain wavelength. This key wavelength is ~0.7 μm, which is only slightly influenced by air mass and aerosol content. On the basis of this result, simple relations are proposed to predict monochromatic AOD from pyrheliometric data and vice versa. The accuracy achieved is close to ±0.01 units of AOD at ~0.7 μm, estimated from simultaneous sunphotometer data. The precision required for the estimation of the precipitable water-vapor content is approximately ±0.5 cm.

OCIS codes: 010.0010, 010.1110, 010.1100.

1. Introduction

Aerosol optical depth (AOD) is usually estimated after subtraction of Rayleigh and gaseous optical depths from sunphotometer extinction measurements across a few narrow-wavelength bands.[1] The realization that aerosols of anthropogenic origin may be significantly modifying the Earth's radiation budget[2] has led to the development of sophisticated instruments and methods for the measurement of aerosol optical properties.[3] The effect of aerosols on the optical properties of the atmosphere can also be evaluated from readily available pyrheliometric data.[4–9] For over a century[7] a valuable application in this context has been to trace the impact of major volcanic eruptions in both hemispheres.

There is, however, an essential problem when one tries to interpret pyrheliometric data. This is the fact that the relation of AOD versus wavelength depends on particle size distribution (PSD) and refractive index, which can be highly variable in space and time. Therefore relating pyrheliometric AOD to the monochromatic AOD at any particular wavelength seems uncertain. The easiest way to circumvent this problem is to assume that the relation of AOD versus wavelength is known beforehand and remains invariable.[8,9] Also seen in the literature[7] is the empirical finding that the pyrheliometric AOD is simply equal to the monochromatic AOD at 0.55 μm, multiplied by a certain constant. This constant is, however, dependent on the optical characteristics of the atmospheric aerosol and takes a value of 1–1.7, according to different authors (Ref. 7 and references therein).

In this paper we tackle the question of relating monochromatic to pyrheliometric AOD, by considering that the heart of the problem lies in finding the wavelength at which both AOD's are equal. Blanchet[10] noticed that this wavelength was ~0.7 μm for several different aerosol models. Our results generally agree with this, showing that this key wavelength, in fact, increases slowly and linearly with both air mass and aerosol loading. An analytical description of this result is presented in Section 2, which is well validated with simulated data in Section 3. Simple relations are proposed in order to derive monochromatic AOD from pyrheliometric data, for which an estimation of errors is presented in Section 4. Section 6 presents an experimental validation of the proposed relations, based on the 9-month data set described in Section 5, which comprises simultaneous pyrheliometer and sunphotometer measurements.

2. Theoretical Background

The stepping stone from which panchromatic (panchromatic refers here to the range 0.3–4 μm, such as measured by a pyrheliometer and encompassing over

B. Molineaux and P. Ineichen are with the Group of Applied Physics, University of Geneva, 1211 Geneva 4, Switzerland. N. O'Neill is with the Centre d'Applications et de Recherches en Télédétection, University of Sherbrooke, Quebec, Canada. The email address for B. Molineaux is benoit.molineaux@gap-e.unige.ch.

Received 24 April 1998; revised manuscript received 23 June 1998.

0003-6935/98/307008-11$15.00/0

99% of solar irradiance) and monochromatic optical depths are defined is Bouguer's law of exponential attenuation:

$$I_\lambda = I_{0\lambda} \exp(-m_R\delta_{\mathrm{CDA}\lambda} - m_w\delta_{w\lambda} - m_a\delta_{a\lambda}), \quad (1)$$

where I_λ and $I_{0\lambda}$ are the attenuated and extraterrestrial direct solar irradiances at wavelength λ in watts times inverse meters squared times inverse micrometers, m_R, m_w, and m_a are the optical masses (ratio of slant path to vertical path through the atmosphere); and δ_{CDA}, $\delta_{w\lambda}$, and $\delta_{a\lambda}$ are the monochromatic optical depths for a vertical atmospheric column. The subscripts R, w, a, and CDA represent Rayleigh scattering, water-vapor absorption, aerosol extinction, and clean dry atmosphere extinction. A CDA represents a fictitious atmosphere that comprises only the effects of Rayleigh scattering and absorption by the atmospheric gases other than water vapor. Stratospheric ozone contributes to <10% of Δ_{CDA}, and seasonal variations of typically ±0.1 atm cm were found to entail variations ≤1% on Δ_{CDA}, which was deemed negligible in the present application. This weak contribution eases the requirements on the optical modeling of stratospheric ozone and helps to justify its inclusion in Δ_{CDA}, despite the fact that the wavelength dependence of ozone extinction and its vertical distribution in the atmosphere differ from that of tropospheric gases (also see Section 3).

The same form of equation can be adopted for the atmospheric attenuation of panchromatic direct solar irradiance:

$$I = I_0 \exp(-m_R\Delta_{\mathrm{CDA}} - m_R\Delta_w - m_R\Delta_a), \quad (2)$$

where the optical depths are the panchromatic analogs of the terms in Eq. (1), I is the direct solar irradiance measured with a standard pyrheliometer in watts times inverse meters squared, and we have approximated m_a and m_w by the value of m_R at sea level. Considering the other approximations inherent to Eq. (2) and the fact that we have restricted our analysis to the range $1 < m_R < 6$, this is a negligible source of errors in the present application (see Ref. 11 for a discussion of the errors resulting from this approximation on the optical masses).

Equation (2) is, however, a lot less straightforward than Eq. (1), because the panchromatic optical depths Δ_{CDA}, Δ_w, and Δ_a are all dependent on air mass and, to a small extent, on each other as well. Indeed, for Eq. (2) to be compatible with Eq. (1), we must set, as in Refs. 12 and 13,

$$\exp[-m_R(\Delta_{\mathrm{CDA}} + \Delta_w + \Delta_a)] = \frac{\int_0^\infty I_{0\lambda} \exp[-m_R(\delta_{\mathrm{CDA}\lambda} + \delta_{w\lambda} + \delta_{a\lambda})]\mathrm{d}\lambda}{\int_0^\infty I_{0\lambda}\mathrm{d}\lambda} = \frac{I}{I_0}. \quad (3a)$$

We can also define the aerosol-free components as in Ref. 12:

$$\exp[-m_R(\Delta_{\mathrm{CDA}} + \Delta_w)] = \frac{\int_0^\infty I_{0\lambda} \exp[-m_R(\delta_{\mathrm{CDA}\lambda} + \delta_{w\lambda})]\mathrm{d}\lambda}{\int_0^\infty I_{0\lambda}\mathrm{d}\lambda}, \quad (3b)$$

which leads to

$$\exp(-m_R\Delta_a) = \frac{\int_0^\infty I_{0\lambda} \exp[-m_R(\delta_{\mathrm{CDA}\lambda} + \delta_{w\lambda} + \delta_{a\lambda})]\mathrm{d}\lambda}{\int_0^\infty I_{0\lambda} \exp[-m_R(\delta_{\mathrm{CDA}\lambda} + \delta_{w\lambda})]\mathrm{d}\lambda} = \frac{I}{I_0 \exp[-m_R(\Delta_{\mathrm{CDA}} + \Delta_w)]}, \quad (4)$$

where the numerator is the attenuated direct solar irradiance as measured by a standard pyrheliometer and the denominator is the panchromatic solar irradiance that would be measured if the atmosphere were free of all aerosol attenuation.

The relations between monochromatic and panchromatic aerosol optical depths ($\delta_{a\lambda}$ and Δ_a, respectively,) can be found through the study of the relation between $\delta_{a\lambda}$ and wavelength, which depends on the PSD. The PSD can be described as

$$n(r) = \partial N/\partial r = Nf(r), \quad (5)$$

where $n(r)$ is the number of particles with a radius between r and $r + \partial r$ per unit volume per unit radius increment, N is the total number of particles per unit volume, and $f(r)$ is the relative size distribution normalized to unity, such that $\int_0^\infty f(r)\mathrm{d}r = 1$. Many different size distributions have been used to characterize aerosol polydispersions. Of special interest in the present context is Junge's power law[14]:

$$n(r) = Cr^{-(\nu+1)}, \quad (6)$$

where ν is sometimes called Junge's size parameter and C is a constant that is proportional to N. This law is usually valid within a certain radius range [outside of which $n(r) = 0$], such that N is a finite number given by $N = \int_{r_1}^{r_2} n(r)\mathrm{d}r = (C/\nu)(r_1^{-\nu} - r_2^{-\nu})$.

The log-normal size distribution (LND) is also often used for tropospheric aerosol models[15,16] and is written as

$$f(r) = \frac{1}{\sqrt{2\pi}\ln\sigma}\frac{1}{r}\exp\left\{-\frac{1}{2}\left[\frac{\ln(r/r_n)}{\ln\sigma}\right]^2\right\}, \quad (7)$$

where r_n is the mode radius and σ is related to the standard deviation of the corresponding normal distribution.

We can relate the particulate volume extinction coefficient at altitude z and wavelength λ to the PSD

by summing all contributions from elemental scatterers of size r, number density $N(z)f(r, z)dr$, and scattering cross section $\pi r^2 Q_{ext}$:

$$\gamma_a(\lambda, z) = \pi N(z) \int_0^\infty r^2 Q_{ext}(x, m) f(r, z) dr, \quad (8)$$

where Q_{ext} is the dimensionless Mie extinction efficiency, x is the Mie size parameter ($x = 2\pi r/\lambda$), m is the particulate (complex) index of refraction at wavelength λ, $f(r, z)$ is the relative size distribution at altitude z, and $N(z)$ is the particle number density at altitude z. The dimensionless AOD integrated over the entire atmospheric layer can then be written as

$$\delta_a(\lambda) = \int_0^\infty \gamma_a(\lambda, z) dz = \pi N_{col} \int_0^\infty r^2 Q_{ext}(x, \bar{m}) \bar{f}(r) dr, \quad (9)$$

where $N_{col} = \int_0^\infty N(z)dz$ is the number of particles in a vertical column of unit cross section, $\bar{f}(r) = (1/N_{col}) \int_0^\infty N(z) f(r, z)dz$ is an average relative size distribution weighted over the entire vertical column, and $\bar{m}$ is a representative refractive index for the total aerosol loading and wavelength λ. If the PSD follows a Junge power law, we can easily obtain the following relation by incorporating the limits r_1 and r_2 and by substituting $x = 2\pi r/\lambda$ into Eq. (9)[17]:

$$\delta_a(\lambda) = \pi C \left(\frac{\lambda}{2\pi}\right)^{-\nu+2} \int_{2\pi r_1/\lambda}^{2\pi r_2/\lambda} x^{-\nu+1} Q_{ext}(x, \bar{m}) dx. \quad (10)$$

If the size distribution of Eq. (6) is valid over the range of radius 0–∞, and the refractive index is assumed to be independent of wavelength, then we can write $\delta_a(\lambda) = \delta_a(\lambda_0)(\lambda/\lambda_0)^{-\nu+2}$, which is of exactly the same form as Ångström's widely used expression[18]:

$$\delta_a(\lambda) = \beta \lambda^{-\alpha}, \quad (11)$$

where β is the equivalent AOD at $\lambda_0 = 1$ μm and the wavelength exponent $\alpha = \nu - 2$. Tomasi *et al.*[19] have suggested that the hypothesis made on both the radius range and the refractive index are unrealistic and that actual atmospheric aerosols may lead to results quite different from Eq. (11). A more flexible approximation is to allow α and β to vary somewhat over the solar spectrum such that Eq. (11) is valid for any size distribution.[20] This approach (i.e., that of a spectrally local Ångström relation) was used in the present study to estimate the AOD at ~0.7 μm from sunphotometer measurements at 0.673 and 0.869 μm.

If the log-normal function is used instead of the power law, Eq. (9) can be written as

$$\delta_a(\lambda) = \frac{\pi r_n^2 N_{col}}{\sqrt{2\pi} \ln \sigma} x_n^{-2} \times \exp\left[-\frac{1}{2}\left(\frac{\ln x_n}{\ln \sigma}\right)^2\right] \int_0^\infty x Q_{ext} \times \exp\left[-\frac{1}{2}\left(\frac{\ln x}{\ln \sigma}\right)^2 + \frac{\ln x \ln x_n}{\ln^2 \sigma}\right] dx, \quad (12)$$

where the wavelength dependence (which is included in the term $x_n = 2\pi r_n/\lambda$) cannot easily be separated from the integral as in Eq. (10). From simulated data and from Eq. (12), we found

$$\delta_a(\lambda) = \frac{u + y(\lambda/\lambda_1)}{(\lambda/\lambda_1)^s + t}, \quad (13)$$

where λ is in micrometers and $\lambda_1 = 1$ μm has been added such that the coefficients s, t, u, and y are dimensionless constants for a given aerosol model. These were derived from fits to Mie simulations for several widely used aerosol models (see Table 1 and Fig. 1 for a few examples). The functional form of Eq. (13) was chosen because it supports all the aerosol models we tested and remains compatible with Ångström's widely used Eq. (11), if t and y tend toward zero, as occurs for small particle distributions such as the soot component of Table 1. For all aerosol models considered here, the standard error for the estimate of $\delta_a(\lambda)$ is less than 1% of its Mie value at 0.7 μm and the correlation coefficient R^2 is always >0.99 over the range $0.3 < \lambda < 3$ μm.

If the particle radii are small and the wavelength is sufficiently large, the second term in the numerator disappears and the AOD decreases monotonically with wavelength. This is due to the fact that the Mie efficiency factor Q_{ext} decreases rapidly with wavelength if the Mie size parameter x is always smaller than its value for which Q_{ext} is maximum (see Fig. 2). The aerosol models for which the effective radius is smaller than ~0.2 μm fall into this category (see Table 1). For aerosol models with an effective radius larger than ~0.6 μm and a relatively wide size distribution, the corresponding range of values of $x = 2\pi r/\lambda$ implies that extinction effects predominantly take place on the right of the maximum in Fig. 2 over the range of wavelengths within the solar spectrum. The result, as can be observed for the dustlike and oceanic polydispersions illustrated in Fig. 1, is that the AOD increases slowly with wavelength.

For fresh volcanic aerosols, with intermediate radii and relatively narrow size distributions, significant extinction takes place on both sides of the maximum in Fig. 2, which leads to the curve of AOD versus wavelength illustrated in Fig. 1. The result is that the AOD at $\lambda = 0.7$ μm is close to the panchromatic AOD for all the aerosol models of Table 1, except for the volcanic aerosol, for which a key wavelength of 0.9 μm is more realistic.

Table 1. Coefficients of Eqs. (7) and (13) for Several Single-Mode and Multimodal Log-Normal Aerosol Models[a]

Aerosol Model	r_n (μm)	σ (–)[b]	r_{eff} (μm)	Refractive Index (–)	s (–)	t (–)	u (–)	y (–)
SRA[c]								
1. Dustlike	0.471	2.512	3.9278	$1.50 - 0.0i$	1.45	5.35	4.31	2.33
2. Water soluble	0.0285	2.239	0.1446	$1.50 - 0.0i$	2.00	0.18	0.66	0
3. Soot	0.0118	2.00	0.039	$1.75 - 0.440i$	1.28	0	0.64	0
4. Oceanic	0.30	2.51	0.635	$1.381 - 4.26E\text{-}9i$	1.65	3.16	2.44	1.82
5. Volcanic	0.217	1.77	0.4903	$1.50 - 0.008i$	2.79	1.20	0.86	1.02
6. Continental[d]					1.95	0.17	0.67	0
7. Urban/industrial[e] Shettle and Fenn[f]					1.68	0.11	0.66	0
8. Large rural	0.5	2.512	1.6619	$1.46 - 0.0033i$	1.42	4.59	3.66	2.18
9. Small rural	0.03	2.239	0.1522	$1.47 - 0.0047i$	1.96	0.178	0.67	0
10. Large urban	0.5	2.512	1.6619	$1.443 - 0.0467i$	1.36	3.42	2.71	1.89
11. Small urban	0.03	2.239	0.1522	$1.453 - 0.0463i$	1.66	0.176	0.73	0
12. Oceanic	0.3	2.512	0.9972	$1.443 - 0.0467i$	1.73	3.97	3.14	1.96
13. Rural mix[g]					1.76	0.20	0.74	0
14. Urban mix[h]					1.46	0.22	0.81	0
15. Maritime mix[h]					1.95	0.18	0.68	0

[a]The polydispersions are all normalized to $\delta_a(0.7\ \mu\text{m}) = 1$. The proportions of single-mode models constituting the multimodal models are given as fractions by number. The coefficients s, t, u, and y were obtained from least-squares fitting to Mie simulations for all models except 13–15, which were obtained from simulations with MODTRAN and a relative humidity of <50%. A relative humidity of ~75% was assumed for models 8–12.

[b](–) indicates that the corresponding numbers are dimensionless.

[c]Ref. 16.

[d]Mix of $2.27 \times 10^{-6} \times$ (model 1) + 0.93876 × (model 2) + 0.06123 × (model 3).

[e]Mix of $1.66 \times 10^{-7} \times$ (model 1) + 0.5945 × (model 2) + 0.4055 × (model 3).

[f]Ref. 15.

[g]Mix of 0.000125 × (model 9) + 0.999875 × (model 10).

[h]Mix of +0.000125 × (model 11) + 0.999875 × (model 12).

[i]Mix of 0.99 × (model 10) + 0.01 × (model 13).

Another interesting observation can be made from Fig. 1. This is that the difference between the panchromatic AOD and the monochromatic AOD is strongly dependent on the PSD for all wavelengths that differ significantly from 0.7 μm. This implies that, unless the PSD is known *a priori*, the monochromatic AOD cannot be estimated from pyrheliometric data with any confidence, except near 0.7 μm. This is a serious impediment to the estimation of monochromatic AOD at 1 μm from pyrheliometric data, as illustrated in Ref. 9.

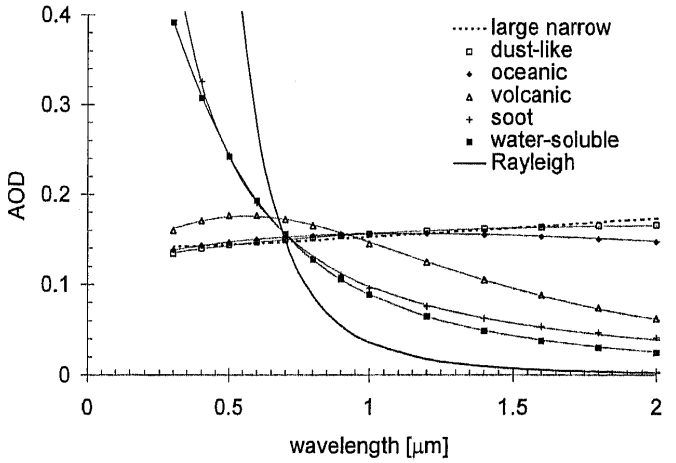

Fig. 1. AOD versus wavelength for the standard reference atmosphere (SRA) aerosol components. All curves are normalized to yield a broadband AOD of 0.15 at air mass 2. The symbols are Mie simulations; the solid curves correspond to Eq. (13) with the coefficients of Table 1. Two of the curves are for comparative purposes only and do not represent realistic aerosol models: (i) the Rayleigh curve, which is nearly proportional to $1/\lambda^4$ and can be considered as the limit of steepest descent for such curves, and (ii) the dotted curve representing Mie simulations for a fictitious narrow size distribution of optically large aerosols (LND with $\sigma = 1.5$, $r_n = 1.7$ μm, and $m = 1.5 - 0i$), which can be considered as near the limit of steepest increase for such curves.

As with the relative size distribution, $f(r)$, it will be convenient to define a relative or normalized AOD, $\hat{\delta}_a$, which is independent of aerosol concentration:

$$\delta_a(\lambda) = A\hat{\delta}_a(\lambda), \tag{14}$$

where A is a dimensionless factor directly proportional to N_{col} and independent of both the wavelength and $f(r)$. We have in fact used $A = \delta_a(0.7\ \mu\text{m})$ for the coefficients of Table 1 above.

The integral of a product of two continuous, posi-

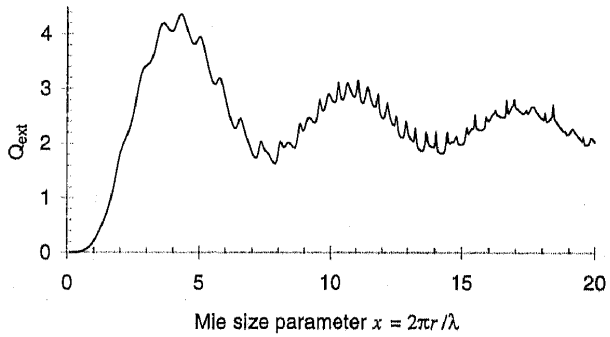

Fig. 2. Mie extinction efficiency (extinction cross section/πr^2) as a function of the Mie size parameter, for a real refractive index of 1.5.

tive functions over a finite range can be written as follows[21]: $\int_a^b f(x)g(x)dx = g(\bar{x})\int_a^b f(x)dx$, where $a < \bar{x} < b$. From this relation we can equate the panchromatic AOD to the monochromatic AOD at a certain wavelength: $\Delta_a = \delta_a(\lambda^*)$, where λ^* lies somewhere in the solar spectrum:

$$\exp(-m_R A\hat{\delta}_a(\lambda^*))\int_0^\infty I_\lambda(a=0)d\lambda = \int_0^\infty I_\lambda(a=0)\exp(-m_R A\hat{\delta}_a(\lambda))d\lambda, \quad (15)$$

where $I_\lambda(a = 0) = I_{0\lambda}\exp[-m_R(\delta_{CDA} + \delta_w)]$ is the spectral direct irradiance emerging from an aerosol-free atmosphere.

Taking a two-term Taylor expansion of the reciprocal of Eq. (15), with $m_R A$ as the variable, yields

$$\frac{1}{\hat{\delta}_a(\lambda^*)} = \frac{1}{\langle\hat{\delta}_a\rangle} + \frac{m_R A}{2}\left[\frac{\langle(\hat{\delta}_a)^2\rangle}{\langle\hat{\delta}_a\rangle^2} - 1\right], \quad (16)$$

where

$$\langle(\hat{\delta}_a)^k\rangle = \frac{\int_0^\infty I_\lambda(a=0)(\hat{\delta}_a)^k d\lambda}{\int_0^\infty I_\lambda(a=0)d\lambda},$$

where the weighted terms $\langle(\hat{\delta}_a)^k\rangle$ are dependent on air mass, as shown in Section 3.

As a first approximation, we neglected the second term on the right-hand side of Eq. (16), used the extraterrestrial spectrum instead of $I_\lambda(a = 0)$, and defined a mean AOD,

$$\bar{\delta}_a = \int_0^\infty I_{0\lambda}\delta_a(\lambda)d\lambda \Big/ \int_0^\infty I_{0\lambda}d\lambda, \quad (17)$$

which is independent of air mass. If we also assume that $\delta_a(\lambda) = \beta\lambda^{-1}$, then the corresponding key wavelength (λ^*) is of course equal to $\beta/\bar{\delta}_a$. We found [from spectral simulations and numerical integration of Eq. (17)] values ranging from 0.69 to 0.72 μm for δ_a(0.5 μm) ranging from 0 to 0.5. This finding, with all the approximations it involves, is in excellent agreement with Fig. 1 above for different aerosol models and is further confirmed by a comparison of $\delta_{a\lambda}$ and Δ_a in Fig. 3. It is also interesting to note that 0.72 μm corresponds to the median of the extraterrestrial spectrum, λ_M, defined from $\int_0^{\lambda_M} I_{0\lambda}d\lambda = \int_{\lambda_M}^\infty I_{0\lambda}d\lambda = (\frac{1}{2})\int_0^\infty I_{0\lambda}d\lambda$.

These results should give a clear answer to the question raised by different authors (Ref. 7 and refs. therein) in trying to relate Δ_a to δ_a(0.55 μm). On the basis of previous evidence, Stothers[7] admits the relation δ_a(0.55 μm) = $k\Delta_a$ and decides on a constant value of $k = 1.6$ for a post volcanic aerosol (for which he assumes that $\delta_{a\lambda} \cong \beta\lambda^{-1}$). He also notes that $(0.55/0.9)^{-1} = 1.6$; i.e., this value of k agrees with the finding of Volz[6] that the key wavelength at which $\delta_{a\lambda} = \Delta_a$ is given by $\int_0^\infty I_{0\lambda}\lambda d\lambda / \int_0^\infty I_{0\lambda}d\lambda \cong 0.9$ μm. If we take the median of the solar spectrum instead of the mean, i.e., 0.7 instead of 0.9 μm, then Stothers should have used $k = (0.55/0.7)^{-1} = 1.3$. Incidentally, the only simultaneous measurements of monochromatic and panchromatic AOD's to which Stothers had access yielded a value of $k = 1.4$. This would mean that the volcanic AOD's at 0.55 μm that Stothers derives from pyrheliometric data are overestimated by at least 20%. There is however a hitch to this argumentation that is in favor of the 0.9-μm value for the key wavelength; it is that the curve of volcanic AOD versus wavelength may be closer to that reported in Fig. 1 than to the $\delta_{a\lambda} \cong \beta\lambda^{-1}$ curve assumed by Stothers. Indeed, the stratospheric AOD measured approximately 1 year after the 1991 Pinatubo eruption is in good agreement with the volcanic aerosol behavior illustrated in Fig. 1 (see Fig. 5 in Russel *et al.*[22]).

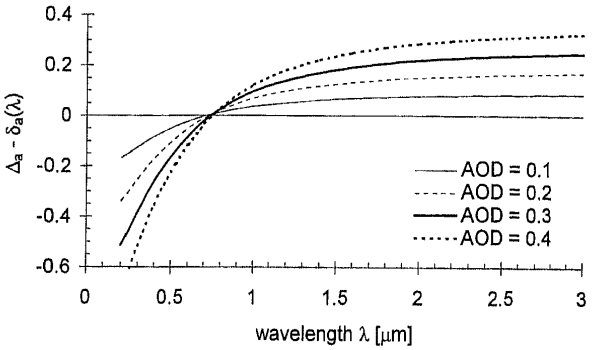

Fig. 3. Difference between panchromatic and monochromatic AOD versus wavelength for different values of AOD (at 0.7 μm). Shettle and Fenn rural aerosol model. Air mass, 2.

3. Simulated Panchromatic Optical Depths

Two radiative transfer codes[23,24] were used to generate spectral direct solar irradiance attenuated by different atmospheric conditions. All simulations were made with the U.S. 1976 standard atmosphere at sea level, with a default stratospheric ozone content of 0.343 atm cm. The first step in the aim of retrieving Δ_a from the measurement of panchromatic direct solar irradiance and Eq. (2) was to find analytical fits for Δ_{CDA} and Δ_w. These were obtained from numerically integrated spectral simulations made with MODTRAN.[23] The following simple expressions were found[25]:

$$\Delta_{CDA} = -0.101 + 0.235m_R^{-0.16}, \quad (18a)$$

$$\Delta_w = 0.112m_R^{-0.55}w^{0.34}, \quad (18b)$$

where w is the precipitable water content in centimeters. The precision of these fits is generally better than 1% when compared with the simulations in the range $1 < m_R < 6$ and $0 < w < 5$ cm.

If the local pressure P is different from $P_0 = 1013.25$ hPa, then Δ_{CDA} can be modeled to a good approximation by simple multiplication of m_R by P/P_0 whenever the term Δ_{CDA} is concerned. The

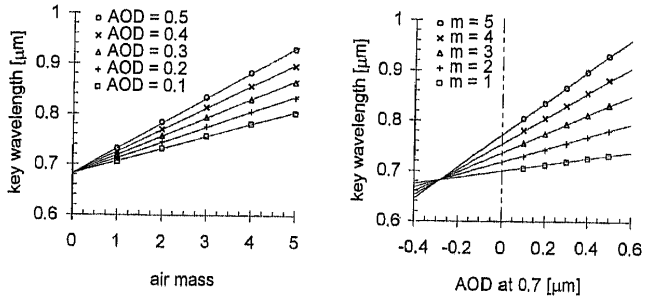

Fig. 4. Key wavelength versus air mass and AOD at 0.7 μm for the Shettle and Fenn rural aerosol mixture. The points are simulated with MODTRAN; the lines correspond to Eq. (19a) with the coefficients of Table 2 for the rural aerosol mixture.

influence of seasonal variations in the stratospheric ozone content on Δ_{CDA} and altitude variations on Δ_w are deemed negligible in the present application.[25]

The spectral codes were then run for different aerosol models to evaluate the dependence of Δ_a on different parameters. The simulations were in excellent agreement with Eq. (16), thus showing that the key wavelength increases linearly with both air mass and aerosol loading, as illustrated for one aerosol model in Fig. 4. Since Δ_a is proportional to $\delta_a(0.7\ \mu m)$, a linear increase of λ^* as a function of Δ_a can also be expected:

$$\lambda^* = \lambda_0 + [B + C\delta_a(0.7\mu m)]m_R, \tag{19a}$$

$$\lambda^* = \lambda_0' + (B' + C'\Delta_a)m_R, \tag{19b}$$

for which the best-fitting coefficients are given in Table 2 for some standard aerosol models. Equation (19a) can be used to predict panchromatic direct solar irradiance from sunphotometer data, whereas Eq. (19b) was used to predict monochromatic AOD's from pyrheliometric data, as illustrated in Section 4.

4. Estimation of Errors

The modeling errors made in estimating $\delta_a(\lambda^*)$ from Δ_a are essentially the result of errors made in estimating λ^*. These can be assessed by differentiation of Eq. (13):

$$\frac{d\delta_a(\lambda)}{\delta_a(\lambda)} \cong \frac{d\lambda}{\lambda}\left(\frac{y}{y + u\lambda^{-1}} - \frac{s}{1 + t\lambda^{-s}}\right), \tag{20}$$

where the differentials $d\delta_a$ and $d\lambda$ represent small errors on $\delta_{a\lambda}$ and λ. The relative errors obtained with Eq. (20) are given in the second-to-last column of Table 2. These errors, however, assume that the atmospheric aerosol size distribution is known beforehand. The uncertainty in the estimation of monochromatic AOD from pyrheliometric data induced by a poor choice of aerosol model are given in the last column of Table 2. These were estimated by use of the coefficients of the standard reference atmosphere (SRA) continental aerosol model for all the aerosol models of Table 2, thus inducing an error in the estimation of the key wavelength. The actual AOD at this wavelength was then compared with Δ_a, and the root mean square difference between the actual and estimated AOD's is reported in Table 2. Only the case of a volcanic aerosol model, with a key wavelength closer to 0.9 μm than to 0.7 μm, results in errors larger than 0.01 units of monochromatic AOD at 0.7 μm. The SRA dustlike model, for which the AOD is quasi-independent of wavelength over the solar spectrum (see Fig. 1), entails no significant loss of precision. This is an important result, because clouds exhibit a similar behavior.[26] Accordingly, contamination of the pyrheliometric data by thin clouds should be a negligible source of errors in the estimation of monochromatic AOD from pyrheliometric data.

We can assess the instrumental errors made in estimating Δ_a from panchromatic data (which are due to uncertainties in the estimation of Δ_w or the

Table 2. Coefficients of Eq. (19) for a Selection of the Aerosol Models Presented in Table 1

Aerosol Model	λ_0 (μm)	B (μm)	C (μm)	SD (μm)	λ_0' (μm)	B' (μm)	C' (μm)	SD[a] (μm)	Error[b] (%)	Error[c] (–)
SRA[d]										
Continental	0.684	0.017	0.067	0.002	0.674	0.017	0.095	0.002	0.3%	<0.001
Urban/industrial	0.672	0.018	0.068	0.002	0.667	0.018	0.092	0.002	0.3%	0.002
Dustlike	0.719	0.012	−0.043	0.004	0.719	0.012	−0.043	0.004	0.1%	0.003
Volcanic	0.944	0.008	0.045	0.002	0.943	0.008	0.055	0.002	0.2%	0.026
Shettle and Fenn[e]										
Rural mix	0.695	0.016	0.066	0.001	0.685	0.017	0.094	0.004	0.7%	0.004
Urban mix	0.696	0.017	0.062	0.001	0.689	0.018	0.084	0.003	0.5%	0.003
Maritime mix	0.727	0.017	0.048	0.002	0.725	0.018	0.056	0.003	0.3%	0.007

[a]Standard deviation between the value of λ^* deduced from simulations and Eq. (19).

[b]Relative error in the monochromatic aerosol optical depth retrieved from pyrheliometric data, calculated as in Eq. (20), assuming the aerosol size distribution is known *a priori* and the error made in estimating λ^* is equal to the standard deviation of the previous column.

[c]Absolute error in the monochromatic aerosol optical depth retrieved from pyrheliometric data if the aerosol model is not known *a priori* and the coefficients of the continental model are used for all aerosol models. This error was calculated from simulations over the range $1 < m_R < 5$ and $0 < \delta_a(0.7\ \mu m) < 0.3$.

[d]Ref. 16.

[e]Ref. 15.

measurement of I with a pyrheliometer) by taking the differential of Eq. (2) and assuming the differentials can be replaced by small (absolute value) differences, as in Eq. (20):

$$d\Delta_a \cong d\Delta_w + \frac{1}{m_R}\frac{dI}{I} \cong 0.037 m_R^{-0.55} w^{-0.66} dw + \frac{1}{m_R}\frac{dI}{I}, \quad (21)$$

where we have inserted Eq. (18b) for Δ_w and assumed that the error in Δ_{CDA} is negligible. Thus an uncertainty of ± 0.5 cm on w at air mass 2 will yield an uncertainty of approximately ± 0.01 in Δ_a. Similarly, an uncertainty of $\pm 2\%$ in the measurement of I will yield an uncertainty of ± 0.01 in Δ_a at air mass 2.

5. Experimental Data

The results presented in the Section 6 refer to instruments collocated on the top of one of the highest buildings in the center of Geneva, Switzerland. This is a small city (population 340,000) situated at 46.2° N, 6.1° E, altitude 400 m. The climate is much influenced by the surrounding mountains and lake such that rapid weather variations are frequent in all seasons, with, however, long periods of cloudy weather in winter. The data represented here cover the period from 1 September 1996 to 31 May 1997, totaling ~500 h of sunshine.

The Eppley pyrheliometer we used for the measurement of direct irradiance has a standard aperture of 5.7°. The monochromatic AOD's were estimated with Eq. (1) and the measurement of $I_\lambda/I_{0\lambda}$ at several wavelengths with two instruments: (i) a Multifilter rotating shadowband radiometer (MFRSR) instrument,[27] which measures the global and diffuse irradiance (with an automated shadowband subtending an angle of 3.3°), from which the direct irradiance is deduced, and (ii) a handmade sunphotometer purchased from SolData[28] and mounted on an Eppley Sun tracker. This second instrument carries eight sensors, each being equipped with a narrow filter (~10 nm at half-maximum) and having an aperture of 5.7°. Both instruments have filters centered at 0.673 and 0.869 μm, from which the AOD at ~0.7 μm was deduced with a spectrally local Ångström relation (see Section 2).

On-line Langley calibration of the sunphotometers was carried out from the data itself. No statistically significant trend could be deduced for the SolData instrument, whereas the calibration constants of the MFRSR showed a severe decrease over the 9-month period considered here, as illustrated in Fig. 5. The 869-nm channel appeared to be the most reliable and was used here to select the days on which Langley plots appeared feasible. On a selection of days, the calibration constants obtained by pure Langley method were compared with, and confirmed by, those obtained by Forgan's Langley-ratio method[29] and the 869-nm reference. The comparison between three completely independent instruments measuring simultaneously in the same site is our best argument in favor of reliable results. It will be shown however (Section 6, Fig. 6 below) that calibration of the monochromatic instruments was not wholly satisfactory. It should also be noted that Geneva's rapidly varying urban climate is not favorable to Langley calibration. The MFRSR 0.937-μm band was calibrated with the modified Langley-plot method,[30] which showed a similar behavior to Fig. 5, with a high dispersion that was due to unstable humidity conditions.

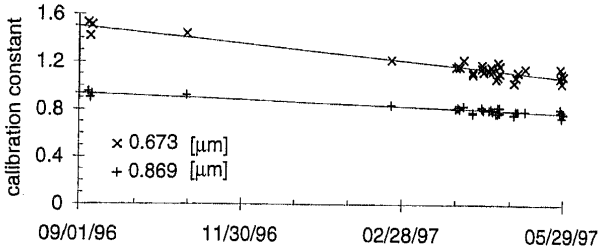

Fig. 5. Drift in the calibration constants (arbitrary units) derived from 30 Langley plots for two of the MFRSR channels. The least-squares linear fits represent the linear calibration values that were used for most of the experimental analysis (see Table 3).

All data considered here are an average of six instantaneous values measured every 10 s, such that one value is recorded per minute. Only the data for which the Sun was higher than 10° above the horizon and the direct irradiance was >100 W m^{-2} are considered here. An independent, automatic quality-control test based on simultaneous measurements of the global and diffuse panchromatic irradiance (measured simultaneously with two other instruments[31]) was applied to the pyrheliometric data. Since the monochromatic and panchromatic data were not collected at exactly the same instant (≤1 min difference), a reduction was necessary in order to eliminate errors that were due to rapidly changing weather conditions. Three time intervals were selected for this purpose (4, 10, and 30 min), from which only one measurement was kept (corresponding to the interval's midpoint). The whole period was discarded if the weather conditions were considered unstable. The criterion for stable conditions was that the Linke turbidity coefficient[4] (T_L) did not vary by more than 0.5 units over a given time interval (where T_L is a dimensionless factor estimated from pyrheliometric data that represents the number of CDA's necessary to produce the actual attenuation; see the list of symbols in Appendix B).

6. Experimental Results

Table 3 shows comparisons between the AOD predicted from pyrheliometric and MFRSR data for a variety of situations: (i) different methods used to calibrate the MFRSR, (ii) different assumed prediction coefficients (or aerosol models), (iii) different estimates of the atmospheric water-vapor content, and (iv) different time intervals over which the weather conditions were judged to be stable. Results obtained with the SolData instrument are not presented in Table 3, because this instrument yielded

Table 3. Comparisons between the AOD at ~0.7 μm Estimated from Panchromatic and Spectral (MFRSR) Data over a 9-Month Period

	Aerosol Model[a]	Interval[b]	Calibration[c]	Water Vapor[d]	No. of Points	Average AOD[e]	MBD[f]	RMSD[f]	SD[f]
1	Urban	10	Const.	Snph.	3757	0.144	−0.004	0.040	0.040
2	Urban	10	Linear	Snph.	3757	0.118	0.010	0.020	0.017
3	Urban	10	Adjust	Snph.	3757	0.124	0.004	0.014	0.013
4	Rural	10	Linear	Snph.	3757	0.118	0.010	0.020	0.017
5	Maritime	10	Linear	Snph.	3757	0.118	0.014	0.023	0.017
6	$\lambda = 0.7$	10	Linear	Snph.	3757	0.118	−0.002	0.024	0.024
7	$\lambda = 0.9$	10	Linear	Snph.	3757	0.118	0.033	0.040	0.024
8	Urban	10	Linear	Meteo	3757	0.118	0.002	0.019	0.018
9	Urban	10	Linear	$w = 0.5$ cm	3757	0.118	0.018	0.028	0.021
10	Urban	10	Linear	$w = +1.0$ cm	3757	0.118	0.002	0.021	0.021
11	Urban	10	Linear	$w = 1.5$ cm	3757	0.118	−0.009	0.022	0.020
12	Urban	4	Linear	Snph.	11,218	0.140	0.008	0.040	0.039
13	Urban	30	Linear	Snph.	996	0.107	0.010	0.019	0.016
14	Urban	30	Adjust	Snph.	996	0.112	0.004	0.013	0.012

[a]The urban, rural, and maritime are those of Shettle and Fenn (see Table 1) modeled as in Eq. (19b) with the coefficients of Table 2. Here $\lambda = 0.7$ or 0.9 means the wavelength at which spectral and panchromatic AOD's are equal is assumed to remain constant, 0.7 or 0.9 μm.

[b]Time interval in minutes between each data point (see text).

[c]Calibration of the MFRSR sunphotometer: (i) Const. means the Langley calibration constants were assumed to remain unchanged over the period of measurements, (ii) linear means the calibration constants obtained from Langley analysis were fitted to a linear decrease over the period of measurements, as in Fig. 4, and (iii) adjust means the Langley calibration constants were adjusted according to the comparisons made with another sunphotometer (see text).

[d]The columnar precipitable water-vapor content was estimated from either (i) sunph. (sunphotometer), extinction in the 0.937-μm band compared to that in the 0.869 μm band, or (ii) meteo, from ground-based ambient temperature and relative humidity (Ref. 32) and (iii) with the assumption that the precipitable water-vapor content remained constant over the 9-month period, 0.5, 1.0, or 1.5 cm.

[e]Average AOD estimated from spectral data at a wavelength of 0.7 μm.

[f]Mean bias, root mean square difference, and standard deviation between the AOD at the key wavelength, ~0.7 μm, estimated from panchromatic data ($\delta_{a\lambda}'$) and spectral data ($\delta_{a\lambda}$): MBD $= (1/n)\Sigma_{i=1}^{n}(\delta_{a\lambda_i}' - \delta_{a\lambda_i})$, RMSD $= [\Sigma_{i=1}^{n}(\delta_{a\lambda_i}' - \delta_{a\lambda_i})^2/(n-2)]^{1/2}$, SD $= (\{\Sigma_{i=1}^{n}(\delta_{a\lambda_i}' - \delta_{a\lambda_i})^2 - [\Sigma_{i=1}^{n}(\delta_{a\lambda_i}' - \delta_{a\lambda_i})]^2/n\}/(n-2))^{1/2}$.

unreliable results over the morning periods (dew problems) and the dispersion was generally large, even in the afternoon.

Errors associated with the calibration of the MFRSR sunphotometer appear to be the determining factor influencing the precision of the results. Assuming a linear decrease as illustrated in Fig. 5 instead of a constant average value brings a spectacular improvement (Table 3, rows 1 and 2). The differences between the AOD's derived from the MFRSR and the pyrheliometer show striking similarities to the differences between the AOD's derived from the MFRSR and SolData sunphotometer (Fig. 6). This is a convincing illustration that the calibration constants of the MFRSR showed a sporadic behavior that cannot be wholly reproduced by the linear decrease of Fig. 5. This was confirmed by the fact that the errors of Fig. 6 are mostly proportional to $1/m_R$ (not illustrated). This is typical of calibration errors, since $d\delta_{a\lambda} \cong (1/m_R)(dI_{0\lambda}/I_{0\lambda})$, as deduced from Eq. (1). We therefore attempted an adjustment of the MFRSR calibration constants by linear fitting over short time periods (approximately 10 days) to the average errors between the two sunphotometers for the 4 months illustrated in Fig. 6 (the other months were characterized by comparatively much smaller errors). Only the afternoon values were considered, in order to avoid dew problems. A small but significant improvement was achieved with this adjustment (rows 3 and 14 of Table 3).

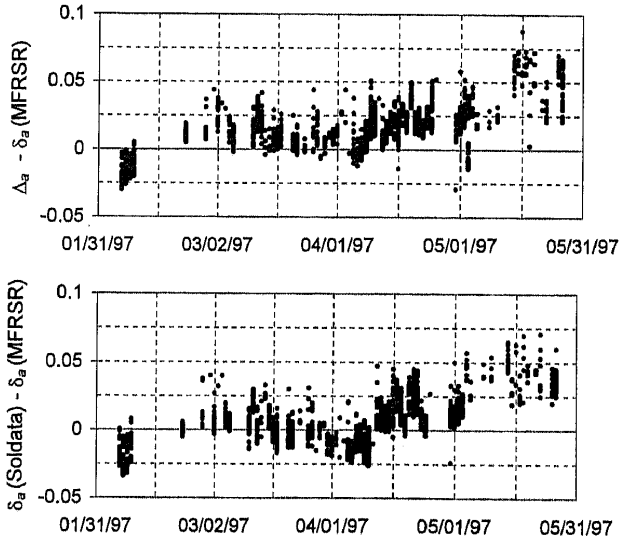

Fig. 6. Top graph, difference between the monochromatic AOD's derived from pyrheliometric data (Δ_a) and MFRSR data (δ_a). Bottom graph, difference between the monochromatic AOD's derived from the SolData and the MFRSR instruments. Afternoon data, 10-min time interval, February–May, 1997. The MFRSR AOD's are calculated with the linear calibration constants (see text).

The choice of aerosol model has only a small influence on the errors obtained here (Table 3, rows 2, 4, and 5). The maritime aerosol model yields the largest errors in this continental, urban site. Assuming the key wavelength takes a fixed value of 0.7 μm yields results that are only slightly worse than those

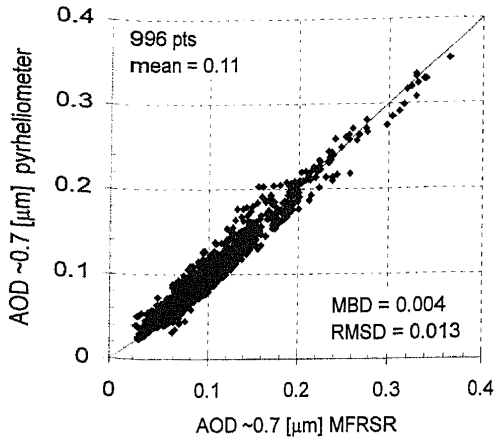

Fig. 7. Comparison between (i) the panchromatic AOD's estimated from pyrheliometric data and (ii) the AOD's retrieved from MFRSR data at the key wavelength of ~0.7 μm, as estimated from Eq. (19b). Instantaneous data selected every 30 min in stable weather conditions covering a 9-month period (see Table 3, row 14).

obtained with Eq. (19). A fixed value of 0.9 μm, as suggested by Refs. 7 and 8, is clearly inappropriate for this data set (Table 3, rows 6 and 7).

Using a value of w deduced from ground-based temperature and humidity measurements[32] yields only a slightly larger dispersion than if water vapor is estimated from the 0.937-μm band (rows 2 and 8 of Table 3). Variations in atmospheric water-vapor content do not appear to have much influence on the dispersion of the results, although an error of 0.5 cm on the average value of w will yield a bias of over 0.01 on the AOD retrieved from panchromatic data (Table 3, rows 9–11).

The best results are obtained with the 30-min time interval (during which the conditions were judged to remain stable). The results for this sampling period and line 14 of Table 3 show that the precision with which the AOD can be derived from pyrheliometric data is surprisingly good, as illustrated in Fig. 7. This is especially relevant if we take into account that the calibration constants of the MFRSR instrument proved to be highly unstable (Figs. 5 and 6). Equation (19a) was also used to estimate panchromatic irradiance from the AOD at 0.7 μm. The comparison of modeled and measured pyrheliometric irradiance is illustrated in Fig. 8, for the same data as in Fig. 7.

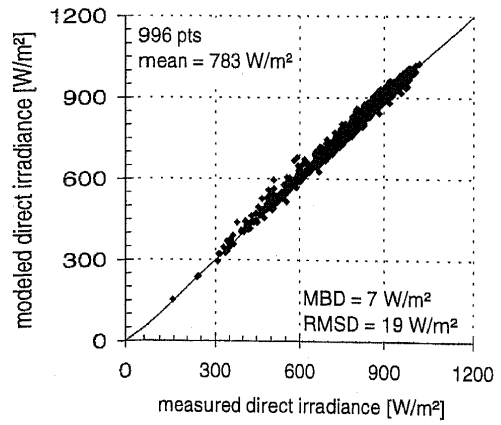

Fig. 8. Comparison between (i) the panchromatic direct irradiance estimated from monochromatic AOD's retrieved from MFRSR data at ~0.7 μm, as estimated from Eq. (19a) and (ii) the direct irradiance measured with an Eppley pyrheliometer. Same data as in Fig. 7.

7. Conclusions

The key wavelength at which panchromatic and monochromatic aerosol optical depths (AOD's) are equal is ~0.7 μm. This conclusion is influenced only slightly by varying air mass or AOD and is representative of most aerosol polydispersions encountered in the terrestrial atmosphere, from submicrometer urban aerosols to cloud droplets. Only the volcanic aerosol model (with a relatively narrow size distribution and an effective radius of 0.5 μm) showed a significantly different behavior, with a key wavelength closer to 0.9 μm. Thus it is possible to estimate the monochromatic (AOD) at approximately 0.7 μm from the measurement of pyrheliometric direct solar irradiance. The precision achieved over a 9-month experimental analysis in an urban climate is close to ±0.01 units of monochromatic AOD at 0.7 μm.

We believe this is an important finding for users of sunphotometer data, owing to two important advantages that are inherent to pyrheliometers: (i) Such data has been currently collected in meteorological stations for years, and (ii) the calibration of a pyrheliometer is straightforward and subject only to small variations, often <1% over several years, whereas sunphotometers are difficult to calibrate and often drift significantly over periods often shorter than a year, as evidenced by the apparent drift of the MFRSR instrument.

These promising results were obtained despite the fact that the measurements were collected in an urban site with a climate subject to rapid variations. An error of ±0.5 cm in the estimation of atmospheric water-vapor content was shown to induce a bias of approximately ±0.01 in the AOD retrieved from panchromatic data, for the conditions of this study. The analytical relations developed here can also be used to estimate panchromatic direct solar irradiance from monochromatic AOD at a single wavelength, with a degree of precision that is close to that of a standard pyrheliometer.

We are grateful to the Ernst and Lucy Schmidheiny Foundation and to the University of Geneva for their sponsorship. Blair Evans is thanked for sharing his Mie code.

Appendix A: List of Acronyms

AOD	aerosol optical depth (monochromatic or panchromatic, as specified),
CDA	clean dry atmosphere,
LND	log-normal (size) distribution,
MFRSR	multifilter rotating shadowband radiometer,
PSD	particle size distribution,
SRA	standard reference atmosphere (see Ref. 16).

Appendix B: List of Symbols in their Order of Appearance

λ wavelengths (μm);
$\delta_a(\lambda)$ or $\delta_{a\lambda}$ monochromatic AOD at wavelength λ (–);
$I_{0\lambda}$, I_λ extraterrestrial and attenuated (i.e., at the Earth's surface) monochromatic direct solar irradiance (W m^{-2} μm^{-1});
I_0, I extraterrestrial and attenuated panchromatic (i.e., integrated over the solar spectrum, from 0 to 4 μm) direct solar irradiance (W m^{-2});
m_R, m_a, m_w relative optical mass, i.e., ratio of slanted to vertical path length for attenuation due to Rayleigh scattering, aerosol extinction and water-vapor absorption (–);
$\delta_{CDA\lambda}$, $\delta_{w\lambda}$, $\delta_{a\lambda}$ clean dry atmosphere, water vapor, and aerosol monochromatic optical depths (–);
Δ_{CDA}, Δ_w, Δ_a panchromatic analogs of the above (–);
w precipitable water vapor in a vertical column above the altitude being considered (cm);
N aerosol number density, i.e., total number of (aerosols per unit volume)
r particle radius (μm);
$n(r)$ differential number density (particles per unit volume per μm), [see Eq. (5)];
$f(r)$ relative size distribution, (particles per μm), [see Eq. (5)];
ν Junge size parameter defined as in Eq. (6) (–);
r_n, σ geometric mean radius (μm) and geometric standard deviation (–) of a LND;
z altitude above sea level (m);
$N(z)$ number of particles per unit volume at altitude z;
$f(r, z)$ relative PSD at altitude z (particles per μm);
$\bar{f}(r)$ average relative PSD weighted over the vertical column (particles per μm);
N_{col} differential abundance or number of particles per unit surface in a vertical column;
Q_{ext} Mie extinction efficiency Q_{ext} = extinction cross section/πr^2 (–);
x Mie size parameter $x = 2\pi r/\lambda$ (–);
m particulate refractive index (–);
$\bar{m}$ representative refractive index for the total aerosol loading (–);
$\gamma_a(\lambda, z)$ particulate volume extinction coefficient for wavelength λ at altitude z (m^{-1} or equivalent);
α Ångström wavelength exponent (–);
β Ångström turbidity factor (μm$^\alpha$);
s, t, u, y constants used in Eq. (13) (–);
RH relative humidity (%);
r_{eff} effective radius defined in Ref. 33 (μm);
A constant that is directly proportional to N_{col} (–);
$\hat{\delta}_a(\lambda)$ normalized or relative monochromatic AOD [see Eq. (14)] (–);
λ^* key wavelength at which $\delta_a(\lambda) = \Delta_a$ (μm);
I or $I_\lambda(a = 0)$ fictitious direct solar panchromatic or monochromatic solar radiation that would arrive at the Earth's surface if the atmosphere were free of aerosols [(W m^{-2}) or (W m^{-2} μm^{-1})];
$\bar{\delta}_a$ mean AOD over the solar spectrum (–);
λ_0, λ_0', B, C, B', C' constants used in Eq. (19) (μm);
T_L Linke turbidity coefficient defined from $I = I_0 \exp[-m_R(\Delta_{CDA}T_L)]$ (–).

References

1. E. G. Dutton, P. Reddy, S. Ryan, and J. J. DeLuisi, "Features and effects of aerosol optical depth observed at Mauna Loa, Hawaii: 1982–1992," J. Geophys. Res. **99,** 8295–8306 (1994).
2. R. J. Charlson, S. E. Schwartz, J. M. Hales, R. D. Cress, J. A. Coackley Jr, J. E. Hansen, and D. J. Hofman, "Climate forcing by anthropogenic aerosols," Science **255,** 423–430 (1992).
3. T. Takamura, Y. Sasano, and T. Hayasaka, "Tropospheric aerosol optical properties derived from lidar, sunphotometer, and optical particle counter measurements," Appl. Opt. **33,** 7132–7140 (1994).
4. F. Linke, "Transmissions-koeffizient und trübungsfaktor," Beitr. Phys. Fr. Atmos. **10,** 91–103 (1922).
5. M. M. Unsworth and J. L. Monteith, "Aerosol and solar radiation in Britain," Q. J. R. Meteorol. Soc. **98,** 778–797 (1972).
6. F. E. Volz, "Atmospheric turbidity after the Agung eruption of 1963 and size distribution of the volcanic aerosol," J. Geophys. Res. **75,** 5185–5193 (1970).
7. R. B. Stothers, "Major optical depth perturbations to the stratosphere from volcanic eruptions: pyrheliometric period, 1881–1960," J. Geophys. Res. **101,** 3901–3920 (1996).
8. J. C. Grenier, A. DeLaCasiniere, and T. Cabot, "A spectral model of Linke's turbidity factor and its experimental implications," Sol. Energy **52,** 303–314 (1994).
9. C. Gueymard, "Turbidity determination from broadband irradiance measurements: a detailed multi-coefficient approach," J. Appl. Meteorol. **37,** 414–435 (1998).
10. J. P. Blanchet, "Application of the Chandrasekhar mean to aerosol optical parameters," Atmos. Ocean **20,** 189–206 (1982).
11. B. W. Forgan, "Bias in a solar constant determination by the Langley method due to structured atmospheric aerosol: comment," Appl. Opt. **27,** 2546–2548 (1988).
12. B. Molineaux and P. Ineichen, "On the broad band transmittance of direct solar radiation in a cloudless sky and its application to the parameterization of atmospheric turbidity," Sol. Energy **56,** 553–563 (1996).
13. J. A. Reagan, P. A. Pilewskie, I. C. Scott-Fleming, B. J. Herman, and A. Ben-David, "Extrapolation of earth-based solar irradiance measurements to exoatmospheric levels for broadband and selected absorption-band observations," IEEE Trans. Geosci. Remote Sens. **GE-25,** 647–653 (1987).
14. C. E. Junge, *Air Chemistry and Radioactivity* (Academic, New York, 1963).
15. E. P. Shettle and R. W. Fenn, "Models for the aerosols of the lower atmosphere and the effect of humidity variations on

their optical properties," Rep. AFGL-TR-79-0214 (U.S. Air Force Geophysics Lab., Hanscom Air Force Base, Mass., 1979).
16. A. Deepak and H. E. Gerber, eds., *Experts Meeting on Aerosols and their Climatic Effects* (World Meteorological Organization, Geneva, 1983), call number WCP-55.
17. H. C. van de Hulst, *Light Scattering by Small Particles* (Dover, New York, 1957).
18. A. K. Ångström, "On the atmospheric transmission of sun radiation and on dust in the air," Geogr. Ann. **11,** 156–166 (1929).
19. C. Tomasi, E. Caroli, and V. Vizale, "Study of the relationship between Ångström's wavelength exponent and Junge particle size distribution exponent," J. Climate Applied Meteor. **22,** 1707–1716 (1983).
20. N. O'Neill and A. Royer, "Extraction of bimodal aerosol-size distribution radii from spectral and angular slope (Ångström) coefficients," Appl. Opt. **32,** 1642–1645 (1993).
21. M. R. Spiegel, *Theory and Problems of Advanced Calculus* (McGraw-Hill, New York, 1973).
22. P. R. Russel, J. M. Livingston, R. F. Pueschel, J. J. Bauman, J. B. Pollack, S. L. Brooks, P. Hamil, L. W. Thomason, L. L. Stowe, T. Deshler, E. G. Dutton, and R. W. Bergstrom, "Global to microscale evolution of the Pinatubo aerosol derived from diverse measurements and analyses," J. Geophys. Res. **101,** 18,745–18,763 (1996).
23. A. Berk, L. S. Bernstein, and D. C. Robertson, "MODTRAN: a moderate resolution model for LOWTRAN 7," GL-TR-89-0122 (1989), updated and commercialized by Ontar Corporation, 9 Village Way, North Andover, Mass. 01845 (1996).
24. C. Gueymard, "SMARTS2, a simple model of the atmospheric radiative transfer of sunshine: algorithms and performance assessment," Rep. FSEC-PF-270-95 (Florida Solar Energy Center, Cape Canaveral, Florida 32920, 1995).
25. B. Molineaux, "Modélisation de la transmission atmosphérique du rayonnement solaire" (Ph.D. dissertation, University of Geneva, Geneva, Switzerland, 1997).
26. D. Deirmendjian, *Electromagnetic Scattering on Spherical Polydispersions* (American Elsevier, New York, 1969).
27. L. Harrison, J. Michalsky, and J. Berndt, "Automated multifilter shadow-band radiometer: an instrument for optical depth and radiation measurements," Appl. Opt. **33,** 5118–5125 (1994).
28. F. Bason, SolData instruments, Linabakken 13, DK-8600 Silkeborg, Denmark, personal communications (1995).
29. B. W. Forgan, "General method for calibrating sunphotometers," Appl. Opt. **33,** 4841–4850 (1994).
30. J. A. Reagan, K. J. Thome, and B. M. Herman, "A simple instrument for measuring columnar water vapor via near-IR differential solar transmission measurements," IEEE Trans. Geosci. Remote Sens. **30,** 825–831 (1992).
31. International Commission on Illumination, *Guide to Recommended Practice of Daylight Measurement* (CIE Central Bureau, Vienna, 1994).
32. J. Wright, R. Perez, and J. Michalsky, "Luminous efficacy of direct irradiance: variations with insolation and moisture conditions," Sol. Energy **42,** 387–394 (1989).
33. J. E. Hansen and L. D. Travis, "Light scattering in planetary atmospheres," Space Sci. Rev. **16,** 527–610 (1974).